Cell, Vol. 83, 1047–1058, December 15, 1995, Copyright © 1995 by Cell Press

The Structure of the G Protein Heterotrimer $G_{i\alpha1}\beta_1\gamma_2$

**Mark A. Wall,* David E. Coleman,* Ethan Lee,†
Jorge A. Iñiguez-Lluhi,† Bruce A. Posner,†
Alfred G. Gilman,† and Stephen R. Sprang*‡**
*Department of Biochemistry
†Department of Pharmacology
‡Howard Hughes Medical Institute
The University of Texas Southwestern Medical Center
Dallas, Texas 75235

Summary

The crystallographic structure of the G protein heterotrimer $G_{i\alpha1}$(GDP)$\beta_1\gamma_2$ (at 2.3 Å) reveals two nonoverlapping regions of contact between α and β, an extended interface between β and nearly all of γ, and limited interaction of α with γ. The major α/β interface covers switch II of α, and GTP-induced rearrangement of switch II causes subunit dissociation during signaling. Alterations in GDP binding in the heterotrimer (compared with α–GDP) explain stabilization of the inactive conformation of α by βγ. Repeated WD motifs in β form a circularized sevenfold β propeller. The conserved cores of these motifs are a scaffold for display of their more variable linkers on the exterior face of each propeller blade.

Introduction

The α and βγ subunits of signal-transducing G proteins are maintained in an inactive state by their mutual association in a heterotrimeric complex (Gilman, 1987; Simon et al., 1991; Bourne et al., 1991; Hepler and Gilman, 1992; Neer, 1995). Within this assembly, the α subunit binds GDP with high affinity, and this interaction is stabilized by βγ. Thus sequestered, neither α nor βγ can interact with downstream effectors. As a consequence of myristoylation, and, additionally, palmitoylation of α and prenylation of γ, heterotrimers are tethered to the inner surface of the plasma membrane. These lipid modifications also stabilize the interaction of α with βγ. In this state, the oligomer is poised to interact with heptahelical transmembrane receptors. The resultant conformational changes in α permit dissociation of GDP and exchange of GDP for GTP. Further conformational changes then result in dissociation of α–GTP from βγ and thus liberation of two activated signal generating molecules. G protein α subunits possess a slow intrinsic GTPase activity that eventually restores the protein to an inactive state in which it readily associates with βγ to complete the cycle.

Mechanistic and structural studies of α subunits and their relatives, particularly members of the p21*ras* superfamily, have yielded a great deal of information about the nature of the guanine nucleotide–driven conformational events that play such important roles in regulation of cell function. Although the conformational changes observed in these molecules differ in detail, the common theme is the loss of crucial interactions between their so-called switch II regions and the γ phosphate of GTP that triggers the structural rearrangements that cause deactivation.

In contrast, it is not known how the G protein βγ subunit complex maintains α in an inactive, GDP-bound state nor how the oligomer is presented to the receptor at the plasma membrane. Furthermore, there are many isoforms of both β and γ subunits. These subunits have extremely high affinity for each other and can be resolved only in the presence of denaturants. However, there is specificity in their interactions with each other and with α (Pronin and Gautam, 1992; Iñiguez-Lluhi et al., 1992), and there is βγ-dictated specificity in the interactions of G protein oligomers with receptors (Kleuss et al., 1992, 1993). The structural bases of these phenomena are unknown. Finally, G protein β subunits are members of a much larger family of proteins that contain multiple copies of a so-called WD or WD40 motif. The structure of such motifs previously has been modeled but not determined (Neer et al., 1994).

We now report the structure of a G protein heterotrimer, composed of α_{i1}, β_1, and γ_2 subunits, at a resolution of 2.3 Å. Oligomers containing α_{i1} are activated by α_2-adrenergic and M_2-muscarinic cholinergic receptors, among others, and α_{i1} is capable of inhibiting certain isoforms of adenylyl cyclase (Taussig et al., 1994). None of the subunits in the crystallized complex contains lipid or other covalent modifications, but the proteins are intact. The structure demonstrates how $\beta_1\gamma_2$ stabilizes the α_{i1}–GDP complex and suggests how the heterotrimer is positioned relative to other components of the signaling pathway in the plasma membrane.

Results and Discussion

Overall Structure of the Heterotrimer

Recombinant nonmyristoylated rat $G_{i\alpha1}$ was synthesized in Escherichia coli and purified as described previously (Lee et al., 1994; Coleman et al., 1994a). Bovine β_1 and γ_2 were coexpressed in Sf9 cells infected with recombinant baculoviruses and purified as a complex (see Experimental Procedures). Cys-68 of the γ_2 subunit was mutated to serine to prevent prenylation of this protein. Heterotrimers were produced by combining GDP–$G_{i\alpha1}$ with $\beta_1\gamma_2$ in a 1:1 molar ratio and were purified by gel filtration. Despite the fact that lipid modifications of both α and γ subunits enhance the affinity of α for βγ, unmodified oligomers can be purified at high concentration and crystallized. Crystals of the heterotrimer grew as tetragonal prisms and belong to space group $P4_3$ with unit cell dimensions of a = b = 84.29 Å, c = 132.39 Å. The asymmetric unit contains a single heterotrimer. The structure was solved by multiple isomorphous replacement-anomalous scattering with two derivatives (Table 1). Diffraction data sets were measured with both synchrotron (native and α_{i1} selenomethionyl derivative) and conventional (samarium derivative) X-ray

Table 1. Statistics for X-Ray Data Collection and Phase Determination

Measurement		Statistic				
Diffraction data		d_{min} (Å)	ΔF/F	Number of Observations (% Completeness)	Redundancy	R_{symm}
Derivative	(λ)					
Native	0.91	2.3	–	35,416 (86.3)	2.9	0.078
Native	0.92	2.9	–	20,172 (95.8)	3.4	0.065
SmOAc	1.54	2.6	17.9	51,206 (91.7)	2.0	0.032
Selenomethione-α	0.91	2.7	16.3	24,751 (97.0)	3.0	0.073

MIR phasing

Derivative	Number of Data[a]	Number of Sites	R_{cullis} Iso	R_{cullis} Anom	F_H/E versus (resolution, Å) (11.2)	(8.2)	(6.2)	(5.1)	(4.3)	(3.7)	(3.2)	(2.9)	Total
SmOAc	19,631	3	0.81	0.5	1.5	1.2	1.6	1.6	1.0	0.8	0.8	0.7	1.0
Selenomethione-α	19,185	6	0.93	0.9	1.0	0.8	1.0	0.8	0.5	0.4	0.4	0.4	0.6
				<FOM>	0.74	0.70	0.74	0.72	0.57	0.48	0.41	0.32	0.47

$R_{symm\,(I)} = \Sigma\Sigma|I_i(hkl) - \overline{I(hkl)}| / \Sigma\Sigma|I_i(hkl)$ $R_{cullis} = \Sigma||F_{PH} \pm |F_P| + |F_{H(calc)}|| / \Sigma|F_H \pm F_P|$ $F_H/E = \left[\Sigma|F_H|^2 / \Sigma|E^2|\right]_{F_{H/E}}$ is the phasing power of the derivative computed by MLPHARE; F_H is the calculated heavy atom scattering amplitude and E is defined as the lack of closure error. F_{PH} is the derivatized protein scattering amplitude, and F_P is the native protein scattering amplitude for any *hkl*. <FOM> is the mean figure of merit. I is reflection intensity. SmOAc is the samarium acetate derivative that was prepared by soaking native crystals in a 1 mM SmOAc solution for 3 hr.

[a] All data from 20.0–2.9 Å.

sources from crystals that were cryoprotected in a liquid nitrogen stream. The native data set extends to a nominal resolution of 2.2 Å, while the structure determination presently includes only data to 2.3 Å. A sample of the Fourier synthesis obtained with experimental phases from isomorphous replacement is compared with a corresponding $2F_{obs} - F_{calc}$ map computed with phases from the refined model at 2.3 Å in Figure 1.

Atomic coordinates have been refined to an R factor of 0.26 (R_{free} = 0.37) for data with $F_{obs} > 2\sigma$ F_{obs} in the 7.0–2.3 Å resolution shell. The model includes residues 2–346 of $G_{i\alpha 1}$ (354 total), 2–340 of β_1 (340 total, including the amino-terminal methionine that is absent in the expressed protein), and 10–46 of γ_2 (71 total), together with one molecule of GDP. Deviations from ideal stereochemistry and the distribution of conformational angles about expected

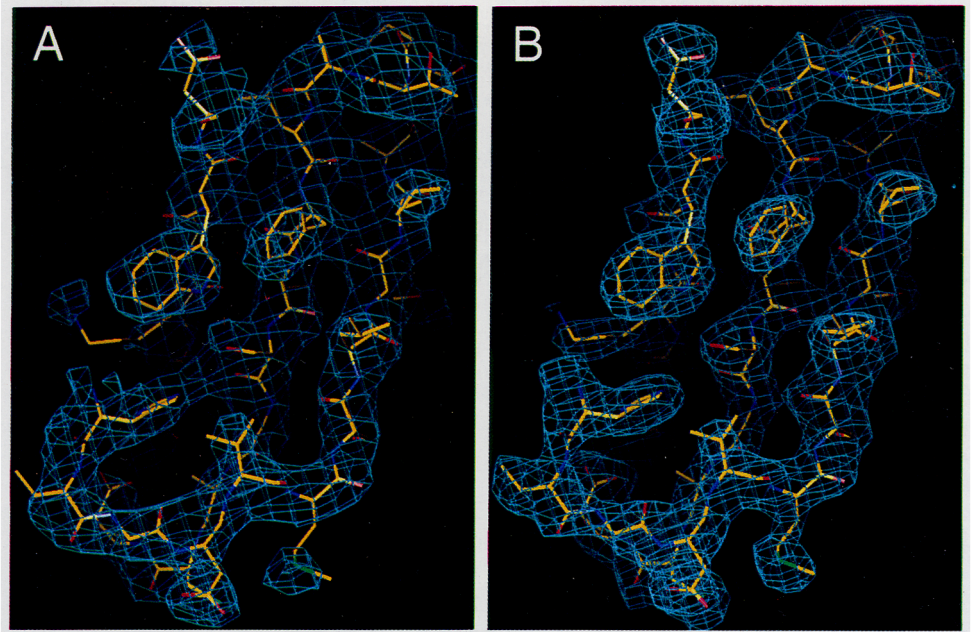

Figure 1. Representative Electron Density

A section of the electron density map in the vicinity of Trp-211 of the β_1 subunit contoured at 1.5 standard deviations above the rms value of the map. The left panel shows the 3.0 Å resolution F_{obs} electron density map computed with phases from multiple isomorphous replacement/anomalous scattering. The refined model is superimposed. The right panel shows the $2F_{obs} - F_{calc}$ electron density map computed over the same region, with phases derived from the refined model.

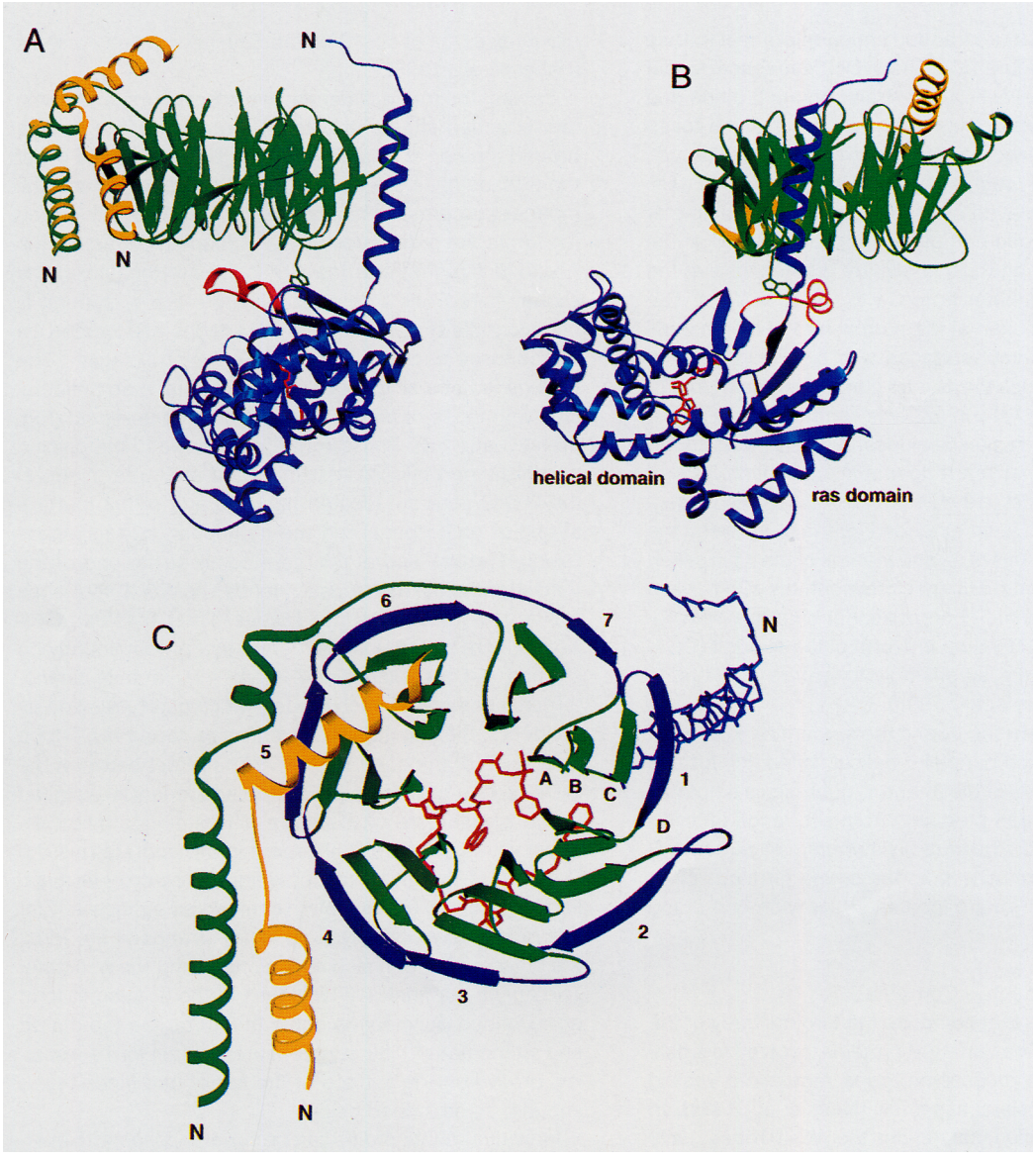

Figure 2. Architecture of the G Protein Heterotrimer

Three views of the heterotrimer with the α_{i1} subunit rendered in blue (the switch II region, residues 199–216, is colored red, as is the molecule of GDP), the β_1 subunit with the side chain of Trp-99 in green, and the γ_2 subunit in yellow. The amino termini of the three subunits are marked with N. The three views are approximately orthogonal. In (C), the polypeptide chains connecting the WD40 cores are colored blue. These contain the D strands of each β blade. The strands of blade 1 are labeled, and each blade is numbered around the periphery of the propeller. The view is taken from the flared end of the β_1 subunit, looking toward the α_{i1} subunit. The backbone atoms of the α_{i1} switch II region and selected side chains are colored red. The backbone atoms of residues 2–35 of the α_{i1} subunit are shown in blue. This figure and Figures 3A, 3B, and 6 were rendered with the program SETOR (Evans, 1993).

values are within the ranges expected for refined X-ray structures determined at moderately high resolution (see Experimental Procedures). Water molecules have not yet been incorporated in the model.

Diffraction from the heterotrimer crystals is characterized by an unusually high Wilson temperature factor of 55 Å^2 for data in the 5–2.3 Å resolution shell. The refined atomic thermal parameters are correspondingly high, averaging 51 Å^2, 52 Å^2, and 56 Å^2 for the α_{i1}, β_1, and γ_2 subunits, respectively. B factors in the cores of α_{i1} and β_1 are in the 35–45 Å^2 range, whereas segments in the amino termini and some loop regions are above 100 Å^2 (see Experimental Procedures). As a consequence of the apparent thermal (and possibly statistical) disorder, the electron density distribution possesses less "atomicity" than would be expected for a 2.3 Å structure determination. Further, although the electron density is continuous, it is not well defined for sections of the chain where B values exceed 80–90 Å^2. The refinement of the model is still in progress.

The heterotrimer (Figures 2A and 2B) is a highly asymmetric structure in which the γ_2 subunit is intimately embedded within β_1, which in turn forms localized but extensive contacts with α_{i1}. The core of the β_1 subunit folds into a toroidal β-propeller domain composed of seven motifs,

each comprising a four-stranded antiparallel sheet that we term a β blade (Figure 2C). The WD40 sequence repeat corresponds to the last (outer) strand of one β blade and the first three (inner) strands of the next. Each of the seven β blades is organized around a narrow central channel, with the β strands roughly parallel with the channel axis. The blades are splayed outward such that the diameter of the channel at one end of the propeller (shown at the top of Figures 2A and 2B) is slightly greater than at the other (average diameter from Cα to Cα is ~12 Å). The α_{i1} subunit is positioned at the narrow end of the channel and forms two contact surfaces with β_1 (Figure 2). The first of these includes the cluster containing the β_2 and β_3 strands and the α_2 helix in α_{i1}. This segment contains the so-called switch II region, residues 199–216, that undergoes conformational rearrangement upon hydrolysis of GTP (Lambright et al., 1994; Mixon et al., 1995). The second contact region is an extended interface between the helical amino terminus of α_{i1} and the side of the β propeller. Most of the segments in α_{i1} that form contacts with β_1 have undergone substantial conformational changes with respect to the free GTPγS-bound form of the subunit (Coleman et al., 1994b) and, surprisingly, to the free GDP-bound form as well (Mixon et al., 1995).

The interface between β_1 and the serpentine γ_2 subunit is extensive, and the parallel α-helical coiled coil formed by the amino termini of the β_1 and γ_2 subunits is a notable feature that had been predicted from sequence analysis (Lupas et al., 1992). The carboxyl terminus of γ_2 (geranylgeranylated in vivo) as well as the amino terminus of α_{i1} (fatty acylated in vivo) are located at the wide end of the β torus.

Architecture of the $\beta_1\gamma_2$ Complex

The WD40 repeats that comprise the toroidal body of the β_1 subunit appear in a variety of proteins involved in signal transduction, RNA processing, gene regulation, vesicle fusion, and cytoskeletal assembly (Neer et al., 1994). In the regular expression that defines the WD40 repeat, only a few residues are well conserved, none of them absolutely. Neer et al. (1994) have represented the WD repeat motif as follows:

$$\{X_{6-94} - [GH - X_{27\pm2} - WD]\}^{N}{}_{4-8}.$$

An amino-terminal sequence of variable length and composition precedes a core of more constant length. Most repeats contain 36–46 residues from WD to WD. Because WD40 proteins contain from four to eight repeats, it was suggested that the repeat itself must fold into a modular structure that is capable of assembling with similar units. This notion is well borne out in the structure of β_1, as is the prediction of β strands in antiparallel arrangement (Neer et al., 1994). The surprising result to emerge here is that the four-stranded antiparallel β motif adopted by the WD40 sequence is common to a diverse group of β propeller proteins (Hunt et al., 1987; Murzin, 1992), which include, among others, neuraminidase (Varghese et al., 1983), galactose oxidase (Ito et al., 1995), methanol dehydrogenase (Xia et al., 1992), and the hemopexin domains (Faber et al., 1995).

To form the toroidal domain of the β_1 subunit, the seven four-stranded sheets (β blades) are nested face to face around the barrel axis (Figure 2C). The first strand (A) of the β blade lines the inner channel of the torus, and the meander progresses outward such that the fourth strand (D) forms the outer edge. The AB loops (connecting the A and B strands) and the CD loops are located at the slightly flared end of the torus, where the γ_2 subunit is bound, while the BC and long DA loops are located on the opposite end that faces the α_{i1} switch II region. The boundaries of a single four-stranded β blade do not coincide with those of an entire WD40 sequence repeat (Figures 2C and 3B). Thus, in the β blade motif, the glycine and histidine residues that mark the amino terminus of the WD40 core are located near the end of the fourth β strand of one repeat, and the tryptophan and aspartate residues at the end of this core occur at the end of the third strand of the next repeat. Hence, the WD40 sequence repeat straddles adjacent β blades. The conserved GH–X–WD cores of the motif contribute predominantly to strands A–C of each blade, while the variable amino-terminal portions of each repeat, which can be viewed as connectors linking the conserved cores, form the CD loop and much of the outer D strand. The offset between the WD40 sequence repeat and the β blade repeat is exploited in the architecture of the torus. The amino-terminal sequence of the first WD40 repeat is incorporated as the D strand of the last β blade, while the carboxy-terminal sequence of the entire protein contributes strands A–C of this blade. Thus, the first and last β strands of the torus are adjacent in the final blade, circularizing the structure. The amino-terminal ~47 residues of the β_1 subunit form an extended polypeptide chain that girds the top (flared end) of the barrel. This segment of the chain forms a shallow groove on the surface of the barrel that binds the γ_2 subunit, as described below.

Individual WD40 motifs can be superimposed with average root mean square (rms) deviations between corresponding Cα atoms ranging from 0.6 Å to 1.2 Å (Figure 3B), within the range expected for homologous sequences of such low identity (Lesk et al., 1986). Most variable in sequence and structures are the D strands, which connect adjacent β blades on the surface of the molecule; these form the linkers between WD40 cores. The AB loops also show structural variability; in blade 3, the AB loop contains a single residue insertion (Figure 3A).

The conserved residues that characterize the WD40 repeat play distinct roles in the organization of its structure (Figure 3C). Most striking among these is the hydrogen-bonded tetrad comprising Trp-*30*, Thr/Ser-*20*, His-*2*, and Asp-*24*. (A numbering system based on the first WD40 motif is adopted here and is distinguished from the ordinal sequence of β_1 by residue numbers in italics; see Figure 3A.) The Thr/Ser-His-Asp network superficially resembles the catalytic triad found in serine proteases. All members of the tetrad are not present in every motif, although Asp-*24* (not the Asp of WD) is an invariant feature; it occu-

A

```
1     MSELDQLRQEAEQLKNQIRDARKACADATLSQITNNIDPVGRIQMRTRRTLRG

SS              |---D---|          |--A-|   |--B-|     |--C--|
45              MRTRRTLRGH..LAKIYAMHWGTDSRLLLSASQDGKLIIWD
84          SYT TNKVHAIPLR..SSWVMTCAYAPSGNYVACGGLDNICSIYN
126   LKTREGN VRVSRELAGH..TGYLSCCRFL DDNQIVTSSGDTTCALWD
171         IET GQQTTTFTGH..TGDVMSLSLAPDTRLFVSGACDASAKLWD
213         VR EGMCRQTFTGH..ESDINAICFFPNGNAFATGSDDATCRLFD
255         LRA DQELMTYSHDNIICGITSVSFSKSGRLLLAGYDDFNCNVWD
299         ALK ADRAGVLAGH..DNRVSCLGVTDDGMAVATGSWDSFLKIWN
Canon.                  |    |    |    |    |    |    |
                        1    5   10   15   20   25   30
```

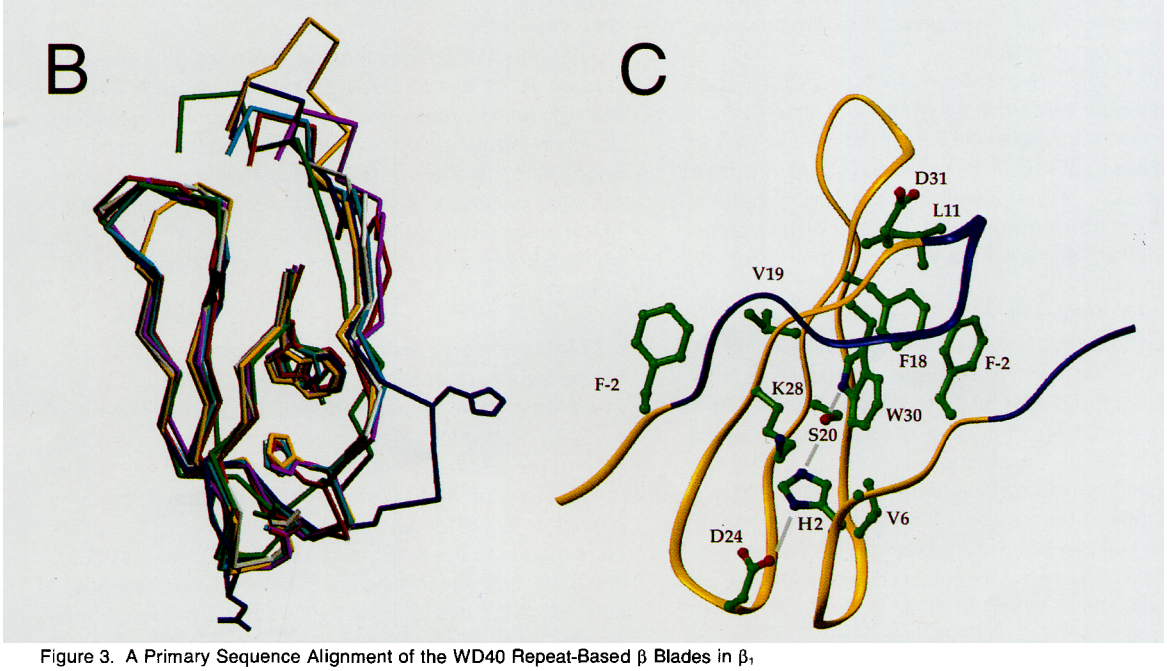

Figure 3. A Primary Sequence Alignment of the WD40 Repeat-Based β Blades in β_1

(A) The alignment is derived from the best three-dimensional superposition of the seven blades. The first row lists the sequence of the amino-terminal residues of β_1 that lie outside of the propeller. The row labeled SS gives the positions of the four β strands of the β blade. The following seven rows show the structure-aligned sequences of the WD40 repeats and are preceeded by the amino-terminal residue number for the repeat. Residues characteristic of the WD40 repeat and contributing to the hydrogen bonded tetrad (see text) are enclosed in boxes. Residues in boldface are highly conserved and serve distinct structural roles in the architecture of the β blade. Residues in red lie within 4.0 Å of the surface of the α_{i1} subunit switch II region in the heterotrimer. Underlined sections define regions that adopt a different conformation than the corresponding residues in blade 1. The last row (labeled Canon) gives a canonical numbering system for residues of the WD40 repeat based on repeat 1.

(B) Residues 45–83 of blade 1 are aligned with corresponding residues in the other six blades. This segment encompasses part of the linker preceding the D strand and the following four strands. The side chains of the conserved His-*2*, Asp-*24*, and Trp-*30* in each repeat are shown (numbering system defined in [A]). Repeats are colored: 1, green; 2, gray; 3, yellow; 4, magenta; 5, cyan; 6, blue; 7, red. The variable amino termini of the repeats are located at the top right.

(C) A backbone representation of blade 4 and the CD linker and strand D of blade five are shown, illustrating the side chains of conserved residues (see [A]). The backbone corresponding to the WD40 core (see text) is colored yellow, and the CD linker and part of the D strand that lies outside of the core are colored blue. Residues are identified with a single-letter code, followed by the ordinal sequence number defined in (A). Note that Phe-2 is represented in both CD linkers. The hydrogen bond network linking Trp-*30*, Ser-*20*, His-*2*, and Asp-*24* is depicted by a gray bar.

pies the central position in a five residue hairpin loop connecting the B and C strands and, in most of the repeats, is hydrogen bonded to a serine or threonine residue at position *26* or to the amide nitrogen of that residue. In most repeats, the aspartate also forms a hydrogen bond to the amide of residue *3* in the DA loop of the previous repeat. The succeeding residue at position *25* adopts a left-handed helical conformation that allows the invariant

aspartate to project into the interior of the hairpin. As shown in Figure 3C, several other conserved residues in the WD40 repeat stabilize the motif and form the interface between adjacent blades.

WD40 repeats 2 and 6 are the most divergent among the seven. Repeat 2 contains no structural analog of His-2. In the linker region leading to WD40 repeat 3 (the loop between the C and D strands of blade 2), there is a four residue insertion. This expanded CD loop forms part of the binding site for the amino-terminal helix of α_{i1}. Both exposed and poorly ordered, this sequence is also a highly preferred site of tryptic cleavage of $\beta\gamma$ (Fong et al., 1986). Blade 6 is unusual in that the variable initial portion of the WD40 repeat (residues 266–270) bears no structural similarity to the corresponding regions of the other repeats. As in repeat 2, there is no structural homolog of His-2. However, in its place is the side chain of Tyr-255 (Tyr-22) of strand C. Residues at the corresponding position 22 in the other repeats contain small side chains, such as serine, alanine, or glycine.

The slightly elliptical channel of the β propeller is lined predominantly by the carbonyl oxygens and amide groups contributed by the A strands of the β blades, as well as by side chains from several cysteine and serine residues. Only a few side chains project into the cavity; those of His-62 and Arg-150 are prominent. The axis of the channel is aimed directly at the switch II helix of the α_{i1} subunit (see Figure 2C).

The first 47 residues of the β_1 subunit form an extended polypeptide chain that wraps around the flared end of the propeller opposite the α_{i1} binding site, embracing its outer surface. The first 27 residues are helical, followed by a bend at residues 28–30 that leads to a second helix terminating at residue 36. Toward the amino terminus, the helix axis diverges from the surface of the β propeller and projects into solvent toward the α-helical domain of the α_{i1} chain. The extended polypeptide is largely supported by its interactions with γ_2, save for contacts near the intrahelical segment with the D strand of blade 5. Residues 38–47 adopt an irregular, extended conformation and contact the D strand of propeller blade 6 before plunging into the propeller as strand D of the last (seventh) blade.

The elongated γ_2 peptide (ordered from residues 10–46) is cradled in a shallow groove formed on one side by the extended amino terminus of β_1 and on the other by polypeptide loops that connect the CD and AB strands of β blades 5 and 6 (see Figure 2C). The direction of the γ_2 chain is parallel to that of the amino terminus of β_1. Of the total 3500 Å^2 of solvent accessible surface of γ_2 (excluding the disordered portions of the chain), ~1300 Å^2 are buried in the interface with β_1 (of a total 2600 Å^2 buried in the $\beta_1\gamma_2$ interface). The amino-terminal residues 10–25 of γ_2 are α helical and pack against the amino-terminal helix of β_1. The two helixes cross at an angle of ~15°, suggestive of a parallel coiled-coil interaction. The coiled-coil packs against the surface of the fourth and fifth blades of the β torus, directly opposite the amino-terminal helix of α_{i1}. The helices of β_1 and γ_2 diverge toward their amino termini. Like β_1, γ_2 projects into solvent toward the α_{i1} subunit, where the terminal residues are unable to form contacts with protein and, presumably therefore, are disordered. Following a short kink at residues 26–29, the following 16 residues of γ_2 fold into an α helix (helix 2) that packs on one side against the CD and AB loops of blade 5. The amino terminus of γ_2 helix 2 is nested against the irregular intrahelical segment of β_1, forming specific hydrogen-bonded contacts. Helix 2 of β_1 and helix 2 of γ_2 run side by side, with γ_2 passing over a hydrophobic cavity lined by the AB and CD loops of blade 6. The region of the β torus in contact with γ_2 corresponds to segments, especially those in blades 5 and 6, that appear to confer the selectivity of β subunits toward individual γ subunits (Pronin and Gautam, 1992; Schmidt et al., 1992; Garritsen and Simonds, 1994; Katz and Simon, 1995). Similarly, the second helix of γ_2 (residues 29–44), which contacts blades 5 and 6, overlaps the 14 residue stretch that determines the selectivity of γ subunits for different β subunits (Spring and Neer, 1994).

Although the carboxy-terminal residues of γ_2 (beyond residue 46) cannot be clearly traced, difference $F_{obs} - F_{calc}$ electron density maps reveal scattered density extending along an irregular path toward the amino terminus of α_{i1}, suggesting that the γ_2-prenyl and α_{i1}-myristoyl moieties of the fully processed chains penetrate the plasma membrane at the same locus. The heterotrimer would be suspended from the membrane by a single tether at its periphery.

α/βγ Interface and βγ-Induced Changes in the Structure of α

The base of the β propeller is positioned directly over the β_2–β_3–α_2 cluster in the p21*ras* domain of the α_{i1} subunit. All but three of the DA (β blades 6 and 7) and BC (blade 6) loops contribute to the α_{i1} contact surface (Figure 4). Almost the entire length of the switch II region of α_{i1}, which corresponds to the β_3–α_2 loop and the α_2 helix (residues 199–216), is buried in the contact with β_1. The hydrophobic core of the contact is organized around Trp-99 of β_1 and Trp-211 of the α_{i1} subunit and also includes the β_1 residues Tyr-59, Met-101, Leu-117, Tyr-145, and Met-188 and the α_{i1} residues Ile-184, Phe-199, Cys-214, Phe-215, and Lys-210. In particular, Trp-99 of the β_1 subunit protrudes into a hydrophobic pocket in the surface of α_{i1}. Although many of the interactions between α_{i1} and β_1 are hydrophobic, the electrostatic potential of the β_1-binding surface is remarkably negative, creating a potential interaction site for cationic intracellular loops of G protein–coupled receptors. Notably, mutation of Trp-136 in the β subunit expressed by Saccharomyces cerevisiae, which corresponds to Trp-99 of the β_1 subunit described here, disrupts interactions between α and βγ and causes constitutive signaling in the mating response pathway (Whiteway et al., 1994). Although the switch II residues 203–209 are located within the subunit interface, the side chains of these residues are poorly ordered and do not form direct contacts with the β subunit. The structure of the α_{i1}/β_1 interface is consistent with the observation that Cys-215 of α_o can be cross-linked with 1,6-bismaleimidohexane to

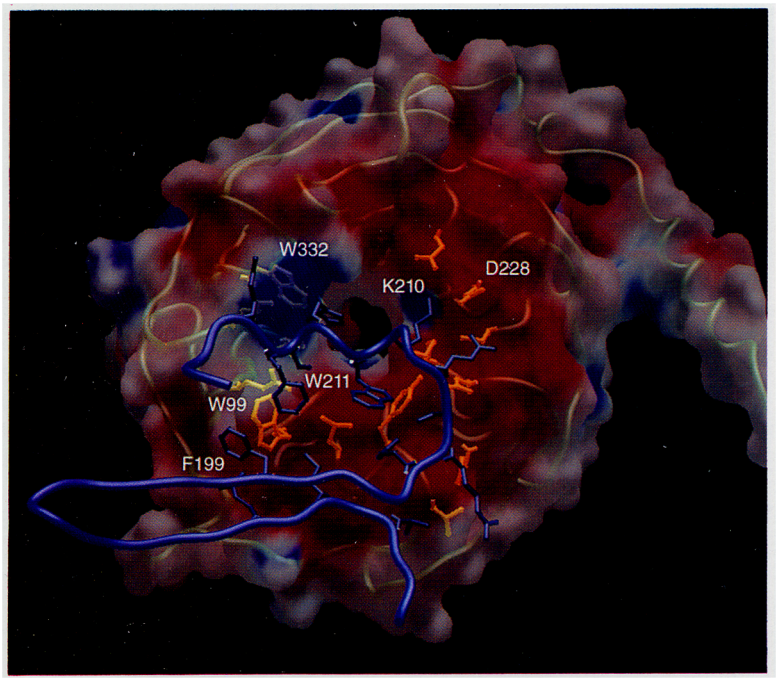

Figure 4. Electrostatic Potential Surface of the β_1 Subunit as Viewed from the α_{i1} Subunit

The backbone trace of β_1 is colored green, and side chains of residues lying within 4 Å of α_{i1} (as indicated in red in Figure 3A) are colored orange. A backbone trace of α_{i1} residues 184–220 (which includes the switch II helix) and the side chains of residues within this segment lying within 4 Å of the β_1 subunit are colored blue. The electrostatic potential surface is shaded from −10 kt/e (red) to +10 kt/e (blue). The electrostatic surface potential and graphics representations were made using GRASP (Nicholls et al. 1991).

either Cys-204 or Cys-271 of β_1 (Thomas et al., 1993; Garcia-Higuera et al., 1996). The two residue pairs are separated by 13 Å and 18 Å, respectively, and are therefore within reach of both reactive moieties of the cross-linking reagent.

The amino-terminal helix of α_{i1} packs across the D strands of the first and seventh blades of β_1 and is flanked by the CD loop of blade 2. The two α_{i1}/β_1 interfaces do not overlap. By itself, the contact region between β_1 and the amino terminus of α_{i1} (residues 2–34) accounts for 950 Å^2 of the total 2500 Å^2 of solvent-accessible surface buried in the entire α_{i1}/β_1 interface.

Formation of the heterotrimer is accompanied by conformational changes in α_{i1} with respect to both its GTPγS–Mg^{2+} and free GDP-bound forms. Both the switch II and the amino-terminal segments of α_{i1} are dynamic components of the interaction. The changes in the switch II region of α_{i1} clearly reveal the mechanism by which hydrolysis of GTP is linked to formation of the complex with $\beta_1\gamma_2$. Liberated from hydrogen-bonded and dipolar interactions with the γ phosphate of GTP, the switch II helix rotates ~120°, exposing the hydrophobic residues Phe-199, Trp-211, and others, to interact with complementary nonpolar pockets in the β subunit as described above (Figure 5). The same rotation also creates two ionic interactions between α_{i1} and β_1: α–Glu-216 forms an ion pair with β–Lys-57, and α–Lys-210 is inserted into a negatively charged pocket formed by Asp-228 and Asp-246 on adjacent loops of β_1.

Formation of the α_{i1}/β_1 interface likewise destabilizes the conformational state of switch II that is required for GTP binding. In the α_{i1}–GTPγS–Mg^{2+} complex, residues 201–209 are α helical. The amino terminus of the helix forms the binding site for the γ phosphate of GTP and positions the catalytic residue Gln-204 for a role in transition state stabilization (Coleman et al., 1994b; Sondek et al., 1994; Privé et al., 1992). To facilitate the "barrel roll" that exposes switch II to the β_1 subunit, the first turn of the α_2 helix unwinds to an extended conformation in which the helix microdipole is dismantled, and Gln-204 becomes disordered. In the absence of $\beta_1\gamma_2$, the switch II region is completely disordered in the α_{i1}–GDP complex (Mixon et al., 1995), indicating that the switch is flexible unless tethered either by contacts with the γ phosphate of GTP or by stabilizing interactions with $\beta_1\gamma_2$.

The conformational changes within switch II are coordi-

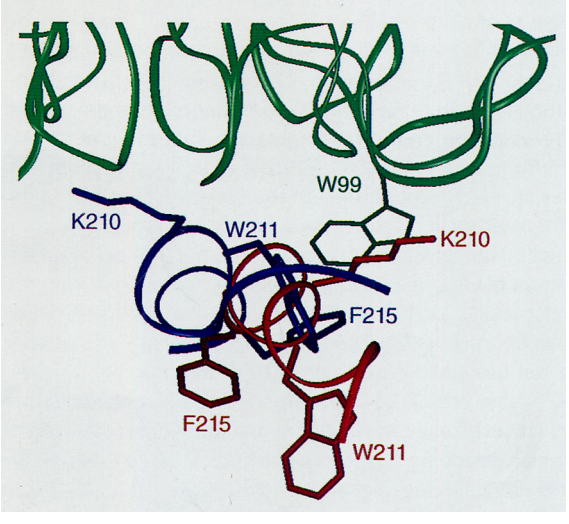

Figure 5. Conformational Differences in the α_{i1} Switch II Helix in the GTP and GDP (Heterotrimeric) Form

Backbone and selected residues for the α_{i1} switch II helix (residues 205–216) are colored red for α_{i1}–GTPγS and blue for the α_{i1}–GDP–$\beta_1\gamma_2$ complex. The β_1 (subunit) is colored green, and Trp-99 is labeled.

nated with a complementary shift of the switch I peptide (residues 178–186) that ultimately traps GDP in the catalytic site of α_{i1} (Figure 6). In the GTP state, Thr-181 of switch I contributes an oxygen ligand to the Mg^{2+} coordination sphere. This structural constraint is removed with the release of Mg^{2+} upon GTP hydrolysis. Switch I is also ejected from the catalytic site to avoid steric interactions with Gly-203 caused by rotation of the switch II helix. This not only repositions Gln-186 and Ile-184 for optimal interaction with β_1, but it also promotes hydrogen bonding and ion pair formation between Arg-178 and Glu-43. As a result, these residues are clasped like a seatbelt over the nucleotide, preventing its diffusion from the catalytic site. Remarkably, Arg-178 adopts a well-ordered conformation only in two states: in the complex with a transition state analog, GDP–AlF_4^-, where it coordinates the aluminum fluoride (and, by inference, the pentacoordinate phosphoryl intermediate of the transition state) (Coleman et al., 1994b), and in the heterotrimeric complex with α_{i1} bound to GDP. This residue is thus crucial both to catalysis and to the positive cooperativity of binding of $\beta\gamma$ and GDP to α (Higashijima et al., 1987), which stabilizes the inactive complex. In this regard, the structures of α_{i1} and α_t are different: in all of the nucleotide-bound states in which it has been crystallized, the corresponding arginine (174) of α_t is well ordered and salt bridged to the nucleotide β phosphate (Noel et al., 1993; Lambright et al., 1994; Sondek et al., 1994).

The amino and carboxyl termini of α_{i1} are also conformationally responsive to guanine nucleotides and $\beta_1\gamma_2$ (Figure 7). In the complex with GTPγS–Mg^{2+}, residues 1–33 are completely disordered, as are residues 345–353 (Coleman et al., 1994b). In crystals prepared with bound GDP, the amino terminus folds into a helix-loop-helix structure that, together with the carboxyl terminus, is organized into a discrete microdomain (Mixon et al., 1995). In the heterotrimer, the amino terminus of α_{i1}–GDP refolds to form a single uninterrupted helical segment extending from residue 33 back to residue 12. Thus extended, the α_{i1} amino terminus is stabilized by favorable interactions with the β propeller of the β_1 subunit. These contacts appear to be crucial to formation of the heterotrimer, since deletion of the amino terminus of α subunits prevents association with $\beta\gamma$ (Fung and Nash, 1983; Taussig et al., 1994). In contrast, the ordered conformation of the carboxyl terminus is destabilized by the loss of interactions with the formerly compact amino terminus. In the heterotrimer, the carboxyl terminus of α_{i1} is exposed for possible interactions with the cytoplasmic domains of appropriate receptors (Conklin and Bourne, 1993). The susceptibility of the heterotrimer to pertussis toxin–catalyzed ADP-ribosylation of α_{i1}–Cys-351 (Neer et al., 1984) is evidence that the carboxyl terminus must be accessible, rather than buried within the compact microdomain observed in free GDP–α_{i1}. However, this proposal does not explain the inability of α_{i1}–GTPγS–Mg^{2+} to be ADP-ribosylated by pertussis toxin.

Implications for Receptor-Mediated Signaling

The structure of the G protein heterotrimer offers a view of its β subunit and thus of a protein constructed from

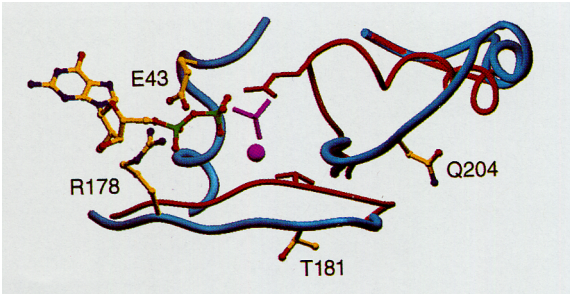

Figure 6. Conformational Changes in the Switch I and Switch II Regions of the α_{i1} Subunit

Selected backbone and side chain residues of α_{i1} are colored as follows: red, α_{i1}–GTPγS–Mg^{2+} (Coleman et al., 1994b); blue, α_{i1}–GDP–$\beta_1\gamma_2$. The GDP molecule in the α_{i1} $\beta_1\gamma_2$ structure is shown, and the γ thiophosphate of GTPγS and the Mg^{2+} found in the α_{i1}–GTPγS structure are colored magenta. In this view, the switch I strand runs along the bottom, and the switch II helix appears in the upper right-hand corner.

WD motifs. As noted above, the conserved core of these repeats contributes predominantly to the three inner β strands (A–C) of the four that comprise the β sheet that forms each blade of the β propeller. The amino-terminal sequence that precedes the core contributes particularly to the outer strand (D) of each preceding blade. Thus, the conserved core can be viewed as a repetitive, circularized scaffold that is used to display more variable sequences about the faces of its compact, symmetrical structure. Variety among members of the family is offered in the choice of the number of repeats and in the size and sequence of the variable outer faces. These structural concepts make sense in the context of the proposal by Neer et al. (1994) that many proteins that contain WD repeats are involved in the formation of multiprotein complexes.

In addition to its own role as a signaling complex, the G protein $\beta\gamma$ subunit maintains associated α subunits in a nonsignaling, GDP-bound state and, at the same time, presents α to the cytoplasmic domains of receptors for activation (Iñiguez-Lluhi et al., 1993; Clapham and Neer, 1993). The mechanism by which the first of these roles is accomplished is clear from the structure of the $\alpha_{i1}\beta_1\gamma_2$ heterotrimer. First, because the effector-binding surface of α encompasses switch II and surrounding regions (Berlot and Bourne, 1992) (as observed in the Raf–Rap complex [Nassar et al., 1995]), as well as amino-terminal sequences (Taussig et al., 1993; Hepler et al., 1995), $\beta\gamma$ may compete directly for effector-binding sites. Further, $\beta\gamma$ stabilizes and sequesters the inactive GDP-bound form of α through specific interactions with the switch II helix. Thus, $\beta\gamma$-induced conformational changes in α both destabilize the GTP-bound form of α and prevent the release of GDP.

Although it is less obvious how receptors catalyze dissociation of GDP from a G protein heterotrimer, it is likely that more than one site of interaction is involved. Sequences in the second and third cytoplasmic loops of heptahelical receptors are important for the selectivity, affinity, or both of receptor–G protein interactions. Similarly, several regions in a G protein heterotrimer are also implicated in this

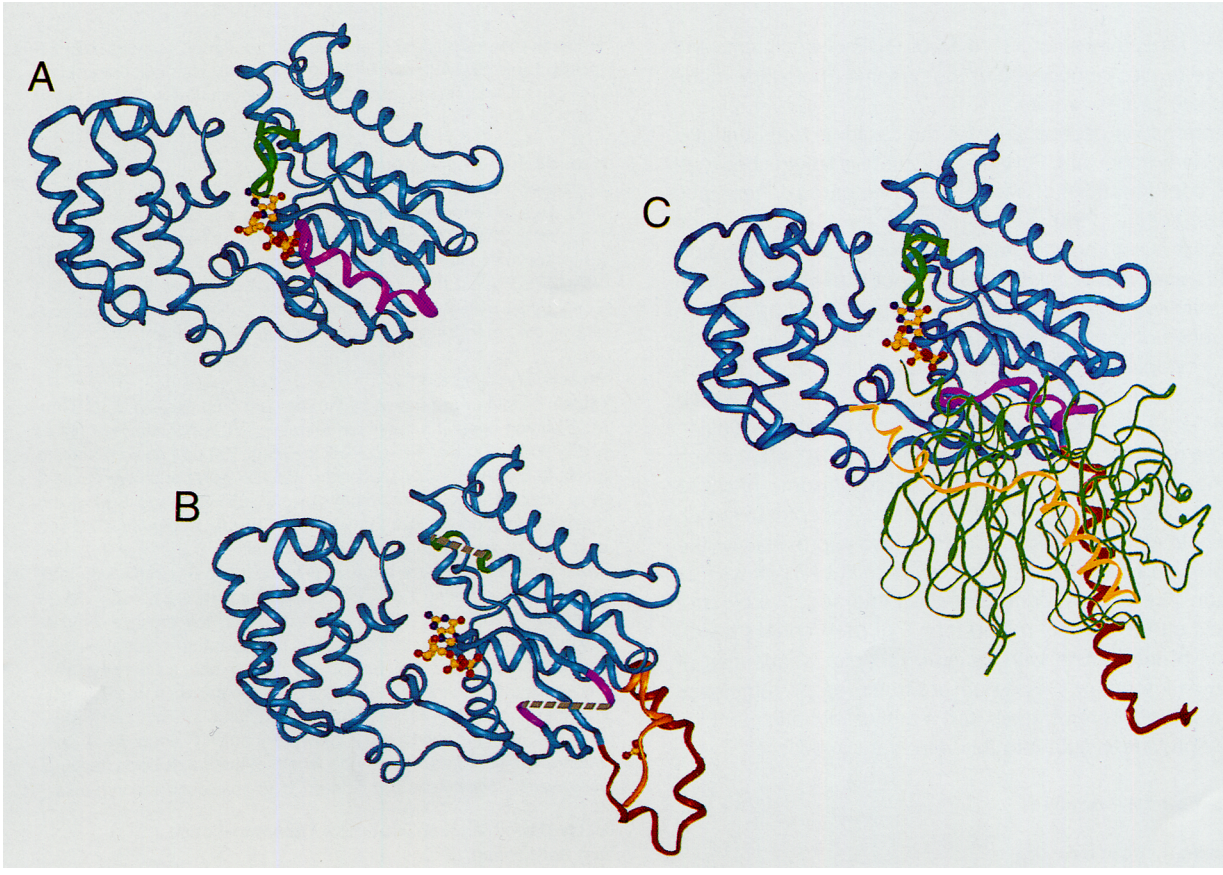

Figure 7. Conformational Changes in the α_{i1} Subunit

Conformational changes in the α_{i1} subunit during the switch from the activated α_{i1}–GTPγS–Mg^{2+} state (Coleman et al., 1994b), through the free, GDP-bound state (Mixon et al., 1995), to the inactive α_{i1}–GDP–$\beta_1\gamma_2$ state described here. Features are colored as follows: blue, α_{i1}; red, α_{i1} amino-terminal residues; brown, α_{i1} carboxy-terminal residues; magenta, α_{i1} switch II; green, α_{i1} switch III; green, β_1; yellow, γ_2.

(A) α_{i1}–GTPγS–Mg^{2+}. The amino and carboxyl termini are disordered in this structure.

(B) α_{i1}–GDP with bound GDP. The carboxy- and amino-terminal residues form a compact microdomain. A sulfate ion bound by the amino-terminal residues is shown. Disordered residues in switch II and switch III are depicted by broken gray lines.

(C) In the $\alpha_{i1}\beta_1\gamma_2$ complex, the amino terminus of α_{i1} is extended to embrace the β_1 subunit.

reaction. The carboxyl terminus of α, which is disordered in the heterotrimer (but which lies near the amino terminus), is clearly important, as judged by the results of mutagenesis and the consequences of its ADP-ribosylation by pertussis toxin (reviewed by Conklin and Bourne, 1993). The amino terminus of α can be labeled with affinity reagents based on receptor-mimetic mastoparans (Higashijima and Ross, 1991) or an appropriate receptor-derived peptide (Taylor et al., 1994). The same peptide also labels the carboxyl terminus of β, most likely in the sixth or seventh blade of the β propeller (R. R. Neubig, personal communication). Finally, it is suspected that the identity of the γ subunit in a given G protein heterotrimer may play an important role in dictating the specificity of receptor–G protein interactions (Kleuss et al., 1993).

The only reasonably secure reference point for interaction of G proteins with the plasma membrane is provided by the lipid modifications of both α and γ subunits. Of interest, the proximity of these modifications suggests that the heterotrimer could be tethered to the membrane at a single point, allowing free access to most of its surface by other signaling molecules. However, it is certainly possible that a cationic or hydrophobic face of the heterotrimer could provide an additional site of interaction. Nevertheless, anchorage to the membrane of the lipid-modified amino and carboxyl termini of α and γ subunits, respectively, would position the "upper" surface of the β propeller (the view in Figure 2A) near the plasma membrane. Loops of the membrane-bound receptor would thus have free access to a large surface of β, much of γ, and the mouth of the tunnel through the propeller. (However, in contrast with the situation that prevails with galactose oxidase (Ito et al., 1995), which also forms a sevenfold β propeller, the diameter of the tunnel in the G protein β subunit is not sufficient to provide substantial access to a polypeptide chain.)

It is likely that direct interactions of receptor with the G protein α subunit are necessary to facilitate dissociation of GDP. This could be accomplished in part by interaction of the receptor with the amino terminus of α, displacing it from the surface of βγ and thus promoting subunit dissociation. However, subunit dissociation alone cannot ex-

plain receptor-enhanced rates of GDP dissociation, and more drastic remodeling of the guanine nucleotide–binding site seems required.

Interaction of receptor with the carboxyl terminus of α is clearly important. Furthermore, there is linkage between the conformations of switch II and the carboxyl terminus (Mixon et al., 1995), although the structural basis for such linkage is not known. Thus, it is conceivable that receptor-enhanced dissociation of GDP could result solely from interactions with the carboxy terminus. Direct interaction of receptor with switch II also seems reasonable. Access of a cytoplasmic receptor loop to switch II might be provided via the cleft between α and β subunits shown on the right side of Figure 2B. This would require extension of the receptor loop from the membrane by 30–40 Å, which is not unreasonable given the length of some of these loops. Of interest, this path of access of receptor to switch II would also bring receptor sequences in proximity to the amino and perhaps the carboxyl termini of α, as well as blade 7 of the β subunit propeller. The negative electrostatic surface in this region (see Figure 4) could provide sites of interaction with cationic receptor sequences of known importance. Solution of structures of complexes of G protein heterotrimers and receptor-mimetic peptides may provide insight into this important question.

Experimental Procedures

Protein Purification

Nonmyristoylated rat $G_{\alpha 1}$ was synthesized in E. coli and purified as described previously (Lee et al., 1994). Large-scale production of $\beta_1\gamma_2$(Cys-68→Ser) was accomplished using a baculovirus expression system. Fall armyworm (Sf9) cells were propagated in IPL-41 medium (GIBCO BRL) supplemented with 10% fetal calf serum (heat inactivated), Pluronic F68 (1%), and gentamicin (Tang et al., 1991). Construction and characterization of the β_1 and γ_2(Cys-68→Ser) baculoviruses has been described previously (Iñiguez-Lluhi et al., 1992). For each purification, Sf9 cells (5 liters) were grown to a density of 2.5 × 10^6 cells/ml and then infected with both the β_1 and γ_2(Cys-68→Ser) baculoviruses (2 pfu per cell per virion). The cells were harvested 60 hr after infection by centrifugation (750 × g), suspended to a density of 5.0 × 10^7 cells/ml in lysis buffer, and subjected to nitrogen cavitation as described previously (Iñiguez-Lluhi et al., 1992). The cell lysate was clarified by centrifugation at 100,000 × g for 30 min at 4°C. All subsequent chromatographic steps were carried out at 4°C on a fast protein liquid chromatography system (Pharmacia) and analyzed by SDS–PAGE. The supernatant (1.5–1.8 g of total protein) was loaded onto two tandem Q-Sepharose HiLoad XK (26/10) anion exchange columns (Pharmacia) equilibrated with 20 mM Tris–HCl (pH 8), 1 mM EDTA, and 3 mM DTT. The protein was eluted using a 1.6 liter gradient of NaCl (0–250 mM) in equilibration buffer, and 20 ml fractions were collected. The appropriate fractions (centered around 150 mM NaCl) were pooled and applied to 50 ml of hydroxylapatite (HTP Biogel, Bio-Rad) packed in an XK 26/20 column (Pharmacia), which had been equilibrated with buffer containing 20 mM Na–HEPES (pH 8), 2 mM DTT, and 100 mM NaCl. The proteins were eluted with a 350 ml gradient (0–75 mM potassium phosphate) in the same buffer, and 6 ml fractions were collected. Fractions containing $\beta_1\gamma_2$(Cys-68→Ser) (centered at ~40 mM potassium phosphate) were pooled, and ammonium sulfate (3.6 M) was added to a final concentration of 1 M. The HTP pool was then loaded onto a phenyl–Superose HR (10/10) column (Pharmacia), equilibrated with buffer containing 20 mM sodium phosphate (pH 7.2), 3 mM DTT, and 1 M ammonium sulfate. The protein was eluted with an 80 ml gradient of decreasing ammonium sulfate (1–0.4 M) in the same buffer, and 1.3 ml fractions were collected. The peak fractions (centered at ~0.6 M ammonium sulfate) were pooled and dialyzed (four times) against storage buffer (20 mM Na–HEPES [pH 8], 1 mM EDTA, 2 mM DTT, 50 mM NaCl). The final preparation (15–20 mg) was concentrated to 20 mg/ml, aliquoted, and stored at −80°C.

Heterotrimer Complex Formation

Separately purified and concentrated α_{i1} and $\beta_1\gamma_2$(Cys-68→Ser) subunits were mixed in a 1:1 molar ratio with 5 mM GDP and incubated for 5 min at 30°C. The complex was loaded on a Superdex 75 column (Pharmacia) equilibrated with buffer containing 150 mM NaCl, 20 mM Na–HEPES (pH 7.0), 1 mM EDTA, 5 mM DTT, and 0.1 mM GDP. Protein was eluted with the equilibration buffer, and fractions containing the heterotrimer were concentrated to 15 mg/ml.

Protein Crystallization

Protein crystals were grown by the hanging drop method at 21°C by equilibration against a reservoir containing 18% polyethylene glycol (PEG) 8000, 100 mM Na–HEPES (pH 7.0), 100 mM sodium acetate (pH 6.4), 0.05% n-β-octyl-glucoside, and 2% 2-propanol. We mixed 3 μl of concentrated (15 mg/ml) $\alpha_{i1}\beta_1\gamma_2$(Cys-68→Ser) and 3 μl of the reservoir solution on glass coverslips. Crystals appeared after 1–3 days and had average dimensions of 1 mm × 0.2 mm × 0.2 mm. The crystals belong to the tetragonal space group $P4_3$ with one heterotrimer in the asymmetric unit. Unit cell dimensions are a = b = 84.29 Å and c = 132.39 Å. The solvent content of the crystals is 50%. Crystals were stabilized for heavy atom derivatization in fresh reservoir solution. Crystals were cryoprotected for frozen data collection by serially soaking them in stabilization solution containing increasing (5%) increments of PEG 400 with the final solution containing 40% PEG 400. Heterotrimer crystals can grow very quickly along the 4_3 axis and are subject to changes in the length of the c axis upon freezing, derivatization, or even slight differences in the precipitation media.

X-Ray Data Collection, Structure Determination, and Refinement

Cryoprotected crystals were mounted in 0.3 mm diameter loops made of unwaxed dental floss fibers and promptly frozen in liquid nitrogen for storage. Crystals were then transferred to a cold nitrogen stream (110 K) for data collection. The crystals diffract with only modest intensity. In the absence of freezing, the diffraction limit drops to ~4.5 Å within minutes, although it is possible to measure data to a limit of 2.5–2.8 Å from a conventional rotating anode source at liquid nitrogen temperatures. For the present study, native data sets were collected at the Cornell High Energy Synchrotron Source (CHESS) A1 beamline, one on each of the two resident charge-coupled device (CCD) detectors. Data for the heterotrimer complex with the selenomethionyl α_{i1} subunit were collected with Fuji HR-V imaging plates at the Brookhaven National Laboratory X25 beamline. Data for the samarium acetate derivative were collected on an RAXIS IIC with mirror-focused CuKα X-rays produced by a Rigaku RU-300 generator. Images were indexed and integrated with the program DENZO, and data were scaled using SCALEPACK (Otwinowski, 1993). Subsequent data manipulations were carried out with the CCP4 package (Collaborative Computing Project, 1994).

Heavy atom refinement and phasing were carried out with MLPHARE (Otwinowski, 1991). The initial multiple isomorphous replacement-anomalous scattering (MIRAS) phases generated a map of limited quality to 3.0 Å. The chain trace for the first five β blades was easily discerned in this map. Main chain density for blades 6 and 7 was broken for two of the four strands in each, but in both cases, at least two of the connecting loops were sufficiently clear to allow the path of the electron density to be traced. The α_{i1} subunit density was also continuous, and its interpretation made easier with reference to preexisting models. Subsequent model building provided phases that, when combined with the original MIRAS phase probability distributions using SIGMAA (Read, 1986) weighting, yielded a map of greater interpretability.

Both electron density maps were skeletonized using the BONES option in MAPMAN program distributed with the program O (Jones and Kjeldgaard, 1993). The model was built into density with O. The α_{i1} subunit was built from the MIRAS map using the activated α_{i1} model (Coleman et al., 1994b) as a guide. Positional grouped B factor and

individual-restrained B factor refinements of the model were carried out with X-PLOR (Brünger, 1992a), using stereochemical restraints of Engh and Huber (1991). After each round of refinement, weighted $2F_o - F_c$ and $F_o - F_c$ maps were generated for manual model building sessions. Simulated annealing slowcool procedures were used after manual model building sessions, and regions of the structure that were originally difficult to interperet were subjected to a simulated annealing omit protocol in which the region in question was omitted from the model undergoing refinement. Several segments of the model have individual restrained B factors in excess of 100 Å^2. These include residues 2–11, 114–115, and 236–238 of α_{i1}, residues 2–9, 129–132, and 267–270 of β_1, and residues 10–23 of γ_2. The free R factor (Brünger, 1992b), computed with 10% of the data randomly selected and removed from refinement, was monitored to evaluate the reliability of convergence. The present R factor is 0.26 (R_{free} = 0.37) for the 35,156 reflections with $F_{obs} > 2\sigma F_{obs}$ in the resolution range 7.0–2.3 Å. The rms deviations from ideal bond distances and bond angles are 0.013 Å and 1.8°, respectively. Main chain φ and ψ torsion angles for 86% of the nonglycine residues fall within most-favored regions of the Ramachandran plot, as defined within the program PROCHECK (Laskowski et al., 1993).

Analysis of the Model

Solvent accessible surface calculations were carried out with a probe radius of 1.5 Å using the method of Lee and Richards (1971) as implemented in a program by T. Richmond and distributed with the CCP4 program library (Collaborative Computing Project, 1994). Electrostatic surface potentials were mapped on the solvent accessible surface with the program GRASP (Nicholls et al., 1991) using the full charge set and default parameters.

Acknowledgments

We are grateful to Albert Berghuis, Jim Naismith, and Ward Coates for assistance with data collection and processing; to Brian Sutton and Orelia Ortiz for assistance with illustrations; to Elliott M. Ross, Eva Neer, and Mark Mixon for helpful discussion; and to Marian Stanzel for skilled technical assistance. This work was supported by National Institutes of Health (NIH) grant DK46371 and Welch Foundation grant I-1229 to (S. R. S.) and by NIH grant GM34497, American Cancer Society grant BE30-O, Welch Foundation grant I-1271, and the Raymond and Ellen Willie Chair of Molecular Neuropharmacology (to A. G. G.).

Received November 16, 1995; revised November 27, 1995.

References

Berlot, C.H., and Bourne, H.R. (1992). Identification of effector-activating residues of $G_{s\alpha}$. Cell *68*, 911–922.

Bourne, H.R., Sanders, D.A., and McCormick, F. (1991). The GTPase superfamily: conserved structure and molecular mechanism. Nature *349*, 117–127.

Brünger, A.T. (1992a). Free R value: a novel statistical quantity for assessing the accuracy of crystal structures. Nature *355*, 472–475.

Brünger, A.T. (1992b). X-PLOR Version 3.1: A System for X-ray Crystallography and NMR (New Haven, Connecticut: Department of Molecular Biophysics and Biochemistry, Yale University).

Clapham, D.E., and Neer, E.J. (1993). New roles for G-protein βγ-dimers in transmembrane signalling. Nature *365*, 403–406.

Coleman, D.E., Lee, E., Mixon, M.B., Linder, M.E., Berghuis, A., Gilman, A.G., and Sprang, S.R. (1994a). Crystallization and preliminary crystallographic studies of $G_{i\alpha 1}$ and mutants of $G_{i\alpha 1}$ in the GTP and GDP-bound states. J. Mol. Biol. *238*, 630–634.

Coleman, D.E., Berghuis, A.M., Lee, E., Linder, M.E., Gilman, A.G., and Sprang, S.R. (1994b). Structures of active conformations of $G_{i\alpha 1}$ and the mechanism of GTP hydrolysis. Science *265*, 1405–1412.

Collaborative Computing Project (1994). The CCP4 suite: programs for protein crystallography. Acta Crystallogr. *D50*, 760–763.

Conklin, B.R., and Bourne, H.R. (1993). Structural elements of Gα subunits that interact with Gβγ, receptors, and effectors. Cell *73*, 631–641.

Engh, R.A., and Huber, R. (1991). Accurate bond and angle parameters for X-ray protein structure refinement. Acta Crystallogr. *A47*, 392–400.

Evans, S.V. (1993). SETOR: hardware lighted by three-dimensional solid model representations of macromolecules. J. Mol. Graphics *11*, 134–138.

Faber, H.R., Groom, C.R., Baker, H.M., Morgan, W.T., Smith, A., and Baker, E.N. (1995). 1.8 Å crystal structure of the C-terminal domain of rabbit serum haemopexin. Structure *3*, 551–559.

Fong, H.K.W., Hurley, J.B., Hopkings, R.S., Miake-Lye, R., Johnson, M.S., Doolittle, R.F., and Simon, M.I. (1986). Repetitive segmental structure of the transducin β subunit: homology with the *CDC4* gene and identification of related mRNAs. Proc. Natl. Acad. Sci. USA *83*, 2162–2166.

Fung, B.K.-K., and Nash, C.R. (1983). Characterization of transducin from bovine retinal rod outer segments. II. Evidence for distinct binding sites and conformational changes revealed by limited proteolysis with trypsin. J. Biol. Chem. *258*, 10503–10510.

Garcia-Higuera, I., Thomas, T.C., Yi, F., and Neer, E.J. (1996). Intersubunit surfaces in G protein αβγ heterodimers: analysis by crosslinking and mutagenesis of βγ. J. Biol. Chem., in press.

Garritsen, A., and Simonds, W.F. (1994). Multiple domains of G protein β confer subunit specificity in βγ interaction. J. Biol. Chem. *269*, 24418–24423.

Gilman, A.G. (1987). G proteins: transducers of receptor-generated signals. Annu. Rev. Biochem. *56*, 615–649.

Hepler, J.R., and Gilman, A.G. (1992). G proteins. Trends in Biochem. Sci. *17*, 383–387.

Hepler, J.R., Biddlecome, G.H., Kleuss, C., Camp, L.A., Hofmann, S.L., Ross, E.M., and Gilman, A.G. (1995). Functional importance of the amino terminus of $G_{q\alpha}$. J. Biol. Chem., in press.

Higashijima, T., and Ross, E.M. (1991). Mapping of the mastoparan-binding site on G proteins: cross-linking of [^{125}I-Tyr3,Cys11]mastoparan to G_o. J. Biol. Chem. *266*, 12655–12661.

Higashijima, T., Ferguson, K.M., Sternweis, P.C., Smigel, M.D., and Gilman, A.G. (1987). Effects of Mg^{2+} and the βγ-subunit complex on the interactions of guanine nucleotides with G proteins. J. Biol. Chem. *262*, 762–766.

Hunt, L.T., Barker, W.C., and Chen, H.R. (1987). A domain structure common to hemopexin, vitronectin, interstitial collagenase and a collagenase homolog. Protein Seq. Data Anal. *1*, 21–26.

Ito, N., Phillips, S.E.V., Stevens, C., Ogel, Z.B., McPherson, M.J., Keen, J.N., Yadav, K.D. S., and Knowles, P.F. (1995). Novel thioether bond revealed by a 1.7 Å crystal structure of galactose oxidase. Nature *350*, 87–90.

Iñiguez-Lluhi, J.A., Simon, M.I., Robishaw, J.D., and Gilman, A.G. (1992). G protein βγ subunits synthesized in Sf9 cells: functional characterization and the significance of prenylation of γ. J. Biol. Chem. *267*, 23409–23417.

Iñiguez-Lluhi, J., Kleuss, C., and Gilman, A.G. (1993). The importance of G protein βγ subunits. Trends Cell Biol. *3*, 230–236.

Jones, T.A., and Kjeldgaard, M. (1993). O Version 5.9 (Uppsala, Sweden: Uppsala University).

Katz, A., and Simon, M.I. (1995). A segment of the C-terminal half of the G-protein β_1 subunit specifies its interaction with the γ_1 subunit. Proc. Natl. Acad. Sci. USA *92*, 1998–2002.

Kleuss, C., Scherubl, H., Hescheler, J., Schultz, G., and Wittig, B. (1992). Different β subunits determine G protein interaction with transmembrane receptors. Nature *358*, 424–426.

Kleuss, C., Scherubl, H., Hescheler, J., Schultz, G., and Wittig, B. (1993). Selectivity in signal transduction determined by γ subunits of heterotrimeric G proteins. Science *259*, 832–834.

Lambright, D.G., Noel, J.P., Hamm, H.E., and Sigler, P.B. (1994). Structural determinants for activation of the α subunit of a heterotrimeric G protein. Nature *369*, 621–628.

Laskowski, R.A., MacArthur, M.W., Moss, D.S., and Thornton, J.M. (1993). PROCHECK: a program to check the stereochemical quality of protein structures. J. Appl. Crystallogr. *26*, 283–291.

Lee, B., and Richards, F.M. (1971). The interpretation of protein structure: estimation of static accessibility. J. Mol. Biol. *55*, 379–400.

Lee, E., Linder, M.E., and Gilman, A.G. (1994). Expression of G protein α subunits in *Escherichia coli*. Meth. Enzymol. *237*, 146–164.

Lesk, A.M., Levitt, M., and Chothia, C. (1986). Alignment of the amino acid sequences of distantly related proteins using variable gap penalties. Protein Eng. *1*, 77–78.

Lupas, A.N., Lupas, J.M., and Stock, J.B. (1992). Do G protein subunits interact via a coiled-coil. FEBS Lett. *314*, 105–108.

Mixon, M.B., Lee, E., Coleman, D.E., Berghuis, A.M., Gilman, A.G., and Sprang, S.R. (1995). Tertiary and quaternary structural changes in $G_{i\alpha 1}$ induced by GTP hydrolysis. Science *270*, 954–960.

Murzin, A.G. (1992). Structural principles for the propeller assembly of β-sheets: the preference for sevenfold symmetry. Proteins *14*, 191–201.

Nassar, N., Horn, G., Herrmann, C., Scherer, A., McCormick, F., and Wittinghofer, A. (1995). The 2.2 Å crystal structure of the Ras-binding domain of the serine/threonine kinase c-Raf-1 in complex with Rap1A-GppNHp. Nature *375*, 554–560.

Neer, E.J. (1995). Heterotrimeric G proteins: organizers of transmembrane signals. Cell *80*, 249–257.

Neer, E.J., Lok, J.M., and Wolf, L.G. (1984). Purificaton and properties of the inhibitory guanine nucleotide regulatory unit of brain adenylate cyclase. J. Biol. Chem. *259*, 14222–14229.

Neer, E.J., Schmidt, C.J., Nambudripad, R., and Smith, T.F. (1994). The ancient regulatory-protein family of WD-repeat proteins. Nature *371*, 297–300.

Nicholls, A., Sharp, K.A., and Honig, B. (1991). Protein folding and association: insights from the interfacial and thermodynamic properties of hydrocarbons. Proteins *11*, 281–296.

Noel, J.P., Hamm, H.E., and Sigler, P.B. (1993). The 2.2 Å crystal structure of transducin-α complexed with GTPγS. Nature *366*, 654–663.

Otwinowski, Z. (1991). Maximum likelihood refinement of heavy atom parameters. In Isomorphous Replacement and Anomalous Scattering, W. Wolf, P.R. Evans, and A.G.W. Leslie, eds. (Warrington, United Kingdom: Science and Engineering Research Council/Daresbury Laboratory), pp. 80–86.

Otwinowski, Z. (1993). Oscillation data reduction program. In Data Collection and Processing, L. Sawyer, N. Isaacs, and S.W. Bailey, eds. (Warrington, United Kingdom: Science and Engineering Council/Daresbury Laboratory), pp. 56–62.

Privé, G.G., Milburn, M.V., Tong, L., deVos, A.M., Yamaizumi, Z., Nishimura, S., and Kim, S.-H. (1992). X-ray crystal structures of transforming p21 ras mutants suggest a transition-state stabilization mechanism for GTP hydrolysis. Proc. Natl. Acad. Sci. USA *89*, 3649–3653.

Pronin, A.N., and Gautam, N. (1992). Interaction between G protein b subunit and γ subunit types is selective. Proc. Natl. Acad. Sci. USA *89*, 6220–6224.

Read, R.J. (1986). Improved Fourier coefficients for maps using phases from partial structures with errors. Acta Crystallogr. *A42*, 140–149.

Schmidt, C.J., Thomas, T.C., Levine, M.A., and Neer, E.J. (1992). Specificity of G protein β and γ subunit interactions. J. Biol. Chem. *267*, 13807–13810.

Simon, M.I., Strathmann, M.P., and Gautam, N. (1991). Diversity of G proteins in signal transduction. Science *252*, 802–808.

Sondek, J., Lambright, D.G., Noel, J.P., Hamm, H.E., and Sigler, P.B. (1994). GTPase mechanism of G proteins from the 1.7-Å crystal structure of transducin α·GDP·AlF_4^-. Nature *372*, 276–279.

Spring, D.J., and Neer, E.J. (1994). A 14-amino acid region of the G protein γ subunit is sufficient to confer selectivity of γ binding to the β subunit. J. Biol. Chem. *269*, 22882–22886.

Tang, W.-J., Krupinski, J., and Gilman, A.G. (1991). Expression and characterization of calmodulin activated (type-1) adenylyl cyclase. J. Biol. Chem. *266*, 8595–8603.

Taussig, R., Iñiguez-Lluhi, J.A., and Gilman, A.G. (1993). Inhibition of adenylyl cyclase by $G^{i\alpha}$. Science *261*, 218–221.

Taussig, R., Tang, W.-J., Hepler, J.R., and Gilman, A.G. (1994). Distinct patterns of bidirectional regulation of mammalian adenylyl-cyclases. J. Biol. Chem. *269*, 6093–6100.

Taylor, J.M., Jacob-Mosier, G.G., Lawton, R.G., Remmers, A.E., and Neubig, R.R. (1994). Binding of an α_2 adrenergic receptor third intracellular loop peptide to G_β and the amino terminus of G_α. J. Biol. Chem. *269*, 27618–27624.

Thomas, T.C., Schmidt, C.J., and Neer, E.J. (1993). G-protein α_o subunit: mutation of conserved cysteines identifies a subunit contact surface and alters GDP affinity. Proc. Natl. Acad. Sci. USA *90*, 10295–10299.

Varghese, J.N., Laver, W.G., and Colman, P.M. (1983). Structure of the influenza virus glycoprotein antigen neuraminidase at 2.9 Å resolution. Nature *303*, 35–40.

Whiteway, M., Clark, K.L., Leberer, E., Dignard, D., and Thomas, D.Y. (1994). Genetic identification of residues involved in association of α and β G-protein subunits. Mol. Cell. Biol. *14*, 3223–3229.

Xia, Z.-x., Dai, W.-w., Xiong, J.-p., Hao, Z.-p., Davidson, V.L., White, S., and Mathews, F.S. (1992). The three-dimensional structures of methanol dehydrogenase from two methylotrophic bacteria at 2.6 Å resolution. J. Biol. Chem. *267*, 22289–22297.